Effects of metal ions concentration on electrodeposited CuZnSn film and its application in kesterite Cu_2ZnSnS_4 solar cells

Received 00th January 20xx,
Accepted 00th January 20xx

DOI: 10.1039/x0xx00000x

www.rsc.org/

Tubshin Hreid[a], Jianjun Li[b], Yi Zhang[b], Henry J. Spratt[c], Hongxia Wang[a*], Geoffrey Will[a*]

In this work, the effects of the concentrations of Cu (II), Zn (II) and Sn (II) ions in electrolytic bath solution on the properties of electrochemically deposited CuZnSn (CZT) films were investigated. The study of the composition of the CZT film has shown that the metallic content (relative atomic ratio) in the film increased linearly with the increase of the metal ion concentration. It is the first time that the relationship of the compositions of the alloy phases in the co-electrodeposited CZT film with the concentration of metal ions was revealed. The results have confirmed that the formantion and content of Cu_6Sn_5 and Cu_5Zn_8 alloy phases in the film were directly controlled by the concentration of Cu (II). SEM measurements have shown that Sn (II) had significant impacts on the film morphology which became more porous as a result of the bigger nucleation size of tin. The changes of surface properties of the films was also confirmed by chronoamperometry characteristic (*i* - *t*) deposition curve. By optimization of the metal ions concentrations in the electrolyte solution, a copper-poor and zinc-rich kesterite Cu_2ZnSnS_4 (CZTS) film was synthesized by sulfurization of the deposited CZT film. The solar cell with the CZTS film showed an energy conversion efficiency of 2.15% under the illumination intensity of 100 mW cm^{-2}.

1. Introduction

The approach based on electrodeposition has been extensively used in practice to fabricate metal/alloy film [1-3] and materials[4, 5] with specific properties for applications due to its advantages of facile, low costing, environmentally friendly and viability for large scale production. Among them, ternary alloys based on CuZnSn (CZT) were mainly employed in industries for decorative and protective purposes in early time.[6] Over recent years, it has been widely used as an essential precursor to synthesize new sustainable photovoltaic materials such as Cu_2ZnSnS_4 (CZTS)[7-10] and $Cu_2ZnSnSe_4$ (CZTSe)[11-14]. Solar cells using electrodeposited Cu_2ZnSnS_4 (CZTS) and $Cu_2ZnSnSe_4$ (CZTSe) with efficiency up to 8.0%[15-18] have been reported.

Generally speaking, electrodeposition of CZT metallic film can be achieved by deposition of Cu/Zn/Sn stacked elemental layers using separate electrolyte solutions containing each metal ion via a multi – steps method[18-22], or by co-deposition using a single solution containing all metal ions in one – step[23-27]. The method based on co-electrodeposition has advantages over the stacked elemental layers method because of its simpler procedure, which is more favorable for high-throughput production. However, compared to the stacked elemental layers approach, it is more challenging to control the co-electrodeposition process of CZT film due to the complexity of the electrolyte system and the different reduction potentials of the metal ions. The simultaneous presence of copper, tin and zinc metal ions with the complexing agent in the electrolyte solution can generate various complex species which may have different solubility and can lead to precipitation in the electrolyte solution[28, 29]. Moreover, in the deposition process, the CZT film deposited from copper, zinc and tin ions may contain the mixture of metals and binary alloys phases such as η-$Cu_{6.26}Sn_5$, Sn and ϫ-$CuZn_5$[30] and Zn, Sn, Cu_6Sn_5 and $CuZn_2$[8]. It has been reported that the alloy phases such as Cu_6Sn_5 and Cu_5Zn_8 in the CZT film have significant effects on the morphology of the CZTS film[10].

Since a high quality CZT precursor film is one of the prerequisites to synthesize CZTS film with desired optical and electronic properties for application in solar cells, it is important to develop effective electrodeposition route for the fabrication of CZT film. According to the generally accepted electrodeposition principles[6], two types of variables can influence the properties of the deposited film: (i)electrolyte solution variables such as the concentration of metal ion, the nature of complexing agent, and the pH of the electrolyte solution; (ii) operational variables such as the electrodeposited current density or potential, deposition temperature and solution mixing. A complexing agent is an important component in an electroplating solution as it can

[a.] *School of Chemistry, Physics and Mechanical Engineering, Science and Engineering Faculty, Queensland University of Technology, Brisbane, QLD. 4001, Australia*
[b.] *Institute of Photoelectronic Thin Film Devices and Technology, Nankai University, Tianjin 300071, China*
[c.] *Central Analytical Research Facility, Institute for Future Environments, Queensland University of Technology, Brisbane, QLD, 4001, Australia*
a* Email: hx.wang@qut.edu.au; g.will@qut.edu.au
Electronic Supplementary Information (ESI) available: [details of any supplementary information available should be included here]. See DOI: 10.1039/x0xx00000x

narrow the gap between different reduction potentials of metals ions and enhance the solubility of metal ions[28]. It can also reduce the grain size of the deposits and improve the homogeneity and roughness of the deposited film[6]. Different complexing agents such as Copper Glo[31, 32], EDTA[33], citric acid [28], and tri-sodium citrate[8, 12-15, 17, 26, 27, 34, 35] have been used in aqueous electrolyte solutions for electrodeposition of CZT films. Among them, tri-sodium citrate is the most widely used one because of its effective complexing abilities to Cu(II), Zn(II) and Sn(II) ions and its environmentally friendly nature[28, 29]. Recently, the effects of the concentration of tri-sodium citrate on the electrodeposition process of CZT film and on the compositions of the deposits were investigated by M. Slupska *et al*[29] while the effects of the applied potentials on the composition of CZT films were studied by C. Gougaud *et al*[28]. However, the report on the influence of the concentration of metal ions on the electrodeposited CZT film using tri-sodium citrate as complexing agent is rare. The concentration of metal ions could have great impact on the CZT film formation through influencing the mass transfer process. Therefore, it is important both fundamentally and practically to distinguish the effects of metal ions concentration on the properties of electrodeposited CZT film in order to gain in-depth understanding of the formation mechanism of CZT film.

Herein, we have investigated the effect of the concentration of each metal ion on the composition, morphology, and crystal structure of the electrodeposited CZT film using static electrolyte solutions containing a constant content of tri-sodium citrate as complexing agent. For the first time, the dependence of the formation of alloys in the co-electrodeposited CZT film on the concentrations of metal ions in the electrolyte was determined quantitatively. A kesterite CZTS film with desired copper-poor and zinc-rich composition was synthesized by controlling the concentrations of the metal ions in the electrolyte solution. The corresponding CZTS solar cell showed energy conversion efficiency of 2.15% under 100 mA cm^{-2}. The research provides new insights into preparation of high quality CZT and CZTS films for solar cell applications through controlling the electrodeposition procedure.

2. Experimental

2.1 Chemicals

Molybdenum coated soda lime glass (Mo/SLG) substrates were ultrasonically cleaned by acetone, ethanol and MiliQ water in sequence for 5 min and dried under nitrogen flow gas. All the chemicals used were analytical agent and supplied by Alfa Aesar unless otherwise stated.

2.2 Preparation of CZT and CZTS films

The electrodeposition of CZT films was implemented with a three-electrode configuration consisting of Mo/SLG substrate working electrode, Pt wire counter electrode and Ag/AgCl/Saturated KCl reference electrode using an electrochemical workstation (VSP-300 Bio-logic). In order to investigate the effects of the concentration of each metal ion on the property of the deposited CZT film, freshly prepared aqueous solutions containing different concentrations of metal ions were used as electrolytic baths. The detailed compositions and the pH value of each solution are shown in Table 1. The solutions containing different concentrations of Cu (II) are named as A series (A1B1C1 – B5). Similarly, the solutions with different concentrations of Zn (II) are labelled as B series (A1B1C1 – B5) and Sn (II) as C series (A1B1C1 – C5) respectively. The starting electrolyte solution is labelled as

Table 1. Chemical composition and pH of electrolyte solutions containing different concentrations of metal ions

Chemical composition of electrolyte solutions					
Series number	$CuSO_4$ (mM)	$ZnSO_4$ (mM)	$SnSO_4$ (mM)	$Na_3C_6H_5O_7$ (mM)	pH
A1B1C1	10.0	10.0	10.0	200	6.2
Different concentrations of copper ion					
A2	12.5	10.0	10.0	200	6.2
A3	15.0	10.0	10.0	200	6.1
A4	17.5	10.0	10.0	200	6.1
A5	20.0	10.0	10.0	200	6.1
Different concentrations of zinc ion					
B2	10.0	12.5	10.0	200	6.2
B3	10.0	15.0	10.0	200	6.2
B4	10.0	17.5	10.0	200	6.2
B5	10.0	20.0	10.0	200	6.2
Different concentrations of tin ion					
C2	10.0	10.0	12.5	200	6.2
C3	10.0	10.0	15.0	200	6.1
C4	10.0	10.0	17.5	200	6.1
C5	10.0	10.0	20.0	200	6.1

A1B1C1 which contains 10.0 mM of each metal ion. For the electrodeposition of copper, zinc and tin individual metal, the electrolyte solution consisted of 10.0 mM each metal sulfate and 200 mM $Na_3C_6H_5O_7{\cdot}2H_2O$. The pH value of each electrolyte solution was adjusted to 6.2 using sulfuric acid. Due to the difficulty of direct deposition of Zn on Mo substrate, the substrate for the electrodeposition of the metal was based on a thin layer of CZT film which was made by electrodeposition of the solution A1B1C1 for 10 minutes. The reduction potential of each metal ion was determined by a linear voltammetry [Fig. S1, Supplementary information]. A negative constant potential of -1.25 V (vs. Ag/AgCl/Saturated KCl) was applied to deposit CZT films for 10 min as well as individual metal films at temperature 26±1 °C. Mo/SLG substrates with an active area of 0.2 cm^2 (circle shape) were used in the electrodeposition for the investigation of the effects of metal ions concentration on CZT films, as well as for electrodeposition of individual metal. A larger area of CZT film (2.2 cm × 2.2 cm) with thickness of ~ 800 nm was prepared for the fabrication of thin film solar cell. The CZTS film was synthesized by sulfurizing the electrodeposited CZT film at 550 °C for 30min in a rapid thermal processing (RTP) furnace (OTF-1200X, MTI) filled with argon (12.0 Torr). The internal temperature of the furnace chamber was heated from ambient temperature to 550 °C in 1 minute.

2.3 Fabrication of CZTS Solar Cell

The CZTS thin film solar cell adopted an architecture of Mo/CZTS/CdS/i-ZnO/ZnO:Al/Ni:Al with an active area of 0.34 cm^2. The cell was made by following the procedure. A 60 nm CdS buffer layer was deposited above the CZTS film using a chemical bath solution containing 1.0 mM $Cd(CH_3COO)_2$, 6.0 mM CH_3COONH_3, 5.0 mM thiourea and 25% ammonia water (5 ml in 250ml bath aqueous solution) by putting the film in the solution for 10 min at 82 ± 2 °C. This was followed by the deposition of the window layer consisting of 50 nm i - ZnO and 500 nm ZnO : Al layers by sputtering. The cell was completed by deposition of Ni/Al grid contact by electron beam evaporation[36].

2.4 Characterization

The composition of the CZT and CZTS films were determined by energy dispersive X-ray spectroscopy (EDS, JEOL 7001F) at an acceleration voltage of 20.0 kV. The relative error of the EDS detector was approximately ±2.0% for Cu, ±2.0% for Zn and ±3.0% for Sn. The surface and cross sectional morphology of CZT and CZTS films were measured by field emission scanning electron microscopy (FMSEM, JEOL 7001F). The X-Ray diffraction patterns of CZT and CZTS films were collected using a PANalytical X'Pert Pro diffractometer operating at 40 kV using Cu Kα radiation in Bragg-Brentano geometry. The relative molar percentages of the crystal phases in the CZT films were determined by refining the XRD diffraction patterns. The Rietveld refinement against the collected XRD patterns was performed using Total Pattern Analysis Solutions *(Topas* V5, Bruker). CuKa5_Berger emission profile was used to describe the incident X-rays. The XRD data between 2θ = 36° and 42° and 71° to 76 ° were excluded in the refinement as these regions contained the intense XRD peaks due to Mo/SLG substrate. A Raman spectrometer (Renishaw inVia Raman microscope) was used to measure the Raman spectrum of the CZTS thin film. The laser excitation wavelength at 532 nm and 785 nm were used in the Raman measurement respectively. The *J-V* characteristic performance of the CZTS solar cell was measured using a solar simulator with AM1.5 spectrum and illumination intensity of 100 mW cm^{-2}.

3. Results and discussion

3.1 Effects of concentration of metal ions on the compositions of CZT films

The dependence of the content of electrodeposited metal (Cu, Zn and Sn) in the film on the concentration of corresponding metals ions is shown in Fig. 1 (a, b and c). The compositional result is an average of three samples prepared under the same condition. For the electrolyte solution with a concentration of 10.0 mM for all the three metal salts (A1B1C1), a CZT film with

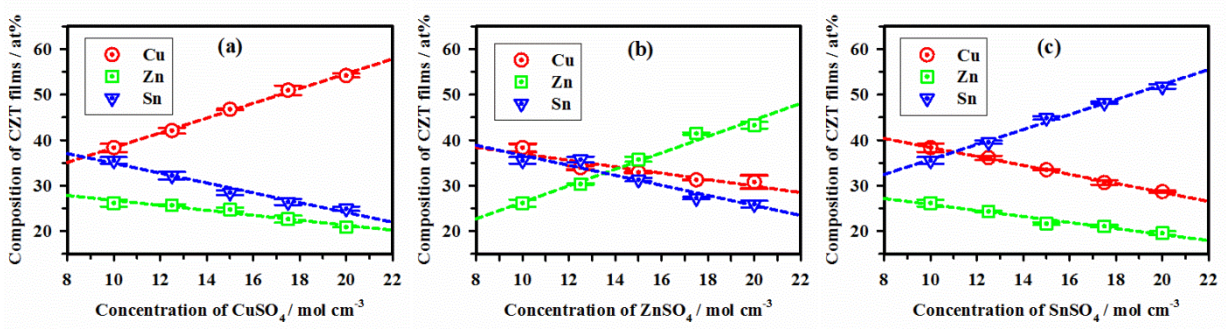

Fig. 1. Dependence of metal content in the electrodeposited CZT films as a function of different concentrations of metal ions (a) Cu (II), (b) Zn (II), and (c) Sn (II) in the electrolyte solutions

a composition (molar ratio) of Cu: Zn: Sn = 1.48: 1.37: 1.00 was obtained. The deviation of the composition from the ratio of the metal ion concentration (1: 1: 1) in the solution suggests the three metals have different deposition rates. Specifically, the deposition rates of the metal ions should be in the order of Cu (II) > Zn (II) > Sn (II). It has been reported that the metal ions can interact with the complexing agent to form non-electroactive metal citrate complexes[29] such as ZnH_2Cit_2 and Zn_2Cit2^{4-} or precipitation components such as $Cu_3SO_4(OH)_4$, $Cu_3SO_4(OH)_6$, Zn_2Cit, $Zn_4(OH)_6SO_4$, $Sn(OH)_2$, which could decrease the effective deposition of metal ions on the substrate. Nevertheless, it is observed that the content of specific metal in the CZT films increases linearly with the increase of the corresponding metal ion concentration in the electrolyte solution while the relative content of the other two metals decrease linearly. It is also observed in Fig. 1 (a, b and c) that the slopes of the plots for the two metals with constant concentration (10.0 mM) in the electrolyte solution are different. This should be attributed to the different deposition rates of the metals and the fact that the electrodeposition of CZT film involves the formation of alloys including Cu_6Sn_5, Cu_5Zn_8 phases instead of pure metals. Therefore, a change of each metal ion concentration would change the surface property of the CZT film, which in turn affects the deposition rate of each metal as shown in the following section.

3.2 Effects of concentration of metal ions on material phases in CZT films

X-ray diffraction was employed to characterize the material phases in the CZT film (Fig. 2 a, b and c). It is found that alloys of Cu_6Sn_5 and Cu_5Zn_8 exist in all the film together with metal tin. The relative contents of the material phases of Cu_6Sn_5, Cu_5Zn_8 and Sn were determined by Rietveld refinement and are correlated with the concentration of each metal ion as shown in Fig. 2 (d, e and f). In the CZT film deposited from the electrolytic solution A1B1C1, the film is dominated by metal Sn phase which accounts for 59.54% while the alloy of Cu_6Sn_5 only accounts for 11.33% of the film. However, as the concentration of Cu (II) in the solution increases, the contents of both Cu_6Sn_5 and Cu_5Zn_8 phases increase while the content of Sn phase decreases rapidly. There is no Sn phase detected by XRD in the film deposited with 17.5 mM of Cu (II) in the electrolyte solution. This indicates the increase of the Cu (II) concentration favors the formation of Cu_6Sn_5 and Cu_5Zn_8 alloys and suppresses Sn in the deposited film. However, with the increase of the concentration of Zn (II) in the electrolyte bath, the content of Cu_5Zn_8 phase remain largely constant and Sn phase slightly increases while Cu_6Sn_5 phase decreases until there is no Cu_6Sn_5 phase when the Zn (II) concentration

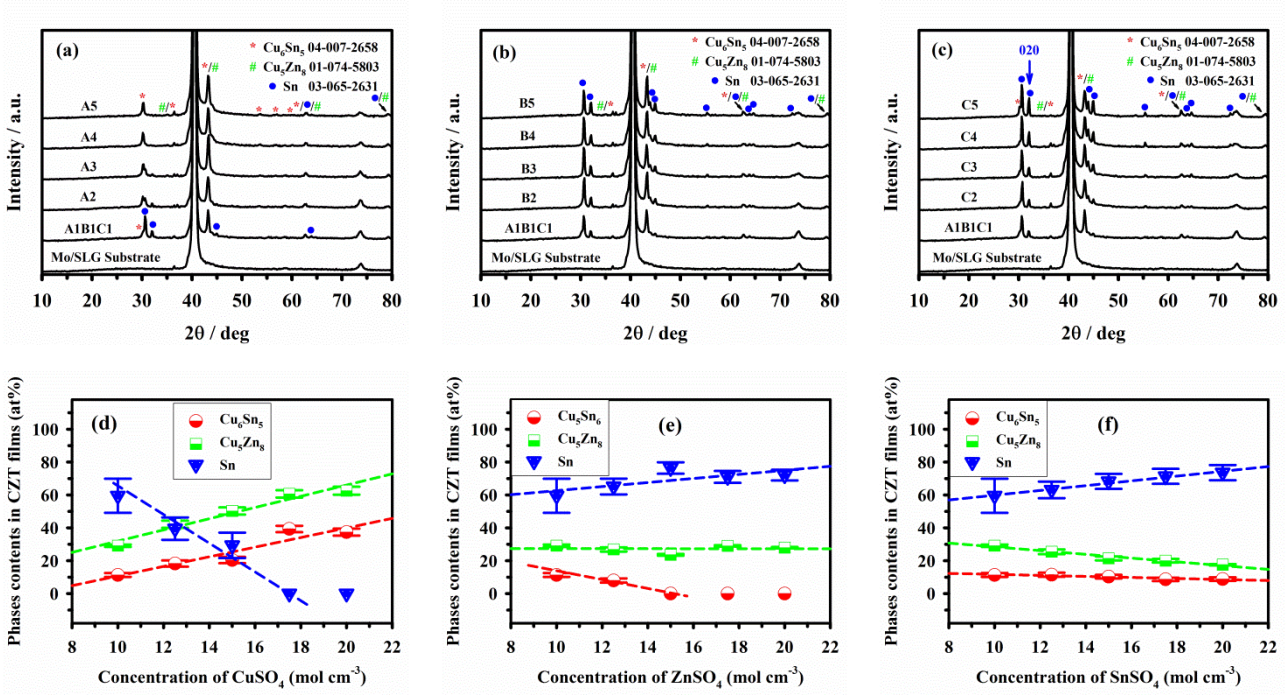

Fig. 2. XRD patterns (a, b, c) and the phases compositions (d, e, f) of the electrodeposited CZT films from electrolyte solutions containing different concentrations of Cu (II) (a, d), Zn (II) (b, e), and Sn (II) (c, f). The contents of each material phase were calculated by Rietveld refinement of the corresponding XRD patterns.

reaches 15.0 mM as illustrated in Fig. 2b. Furthermore, the increase in Sn (II) concentration is found to facilitate the formation of Sn phase while hindering the Cu_5Zn_8 phase and has almost no effects on Cu_6Sn_5, as shown in Fig. 2c**.** The results suggest that formation of both Cu_5Zn_8 and Cu_6Sn_5 alloy phases is determined by the concentration of Cu (II) instead of Zn (II) and Sn (II).

3.3 Effects of concentration of metal ions on morphology of CZT films

The evolution of the morphology of the CZT films deposited from different concentrations of metal ions is illustrated in Fig. 3**.** It is found that the morphology of the CZT films deposited from solutions (A1B1C1 - A5) containing different concentrations of Cu (II) is very similar, indicating the negligible effect of the content of copper on the CZT film morphology. The films are mainly composed of ~ 200 nm crystal grains formed from nano-scaled small particles. In contrast, the morphology of the CZT film changes slightly with the increase of Zn (II) concentration and thus metal Zn in the film**.** As shown in Fig. 3 (A1B1C1 - B5)**,** the increasing content of zinc in the film leads to the more defined spaces between crystal grains and rougher film surface. Meanwhile, the crystal sizes of the grains are increased to more than 200 nm (B4). Bigger grains with size around ~ 300 nm are found in B5. In contrast, the effects of Sn (II) on the CZT film morphology are even more pronounced. When the concentration of Sn (II) increases, the film becomes porous and rougher as illustrated in Fig. 3 (A1B1C1 – C5). The agglomerations of particles are also observed in higher concentrations of Sn (II), as shown in Fig. 3 (C3 – C5). The different morphological behavior induced by the metals ions should be related to the different

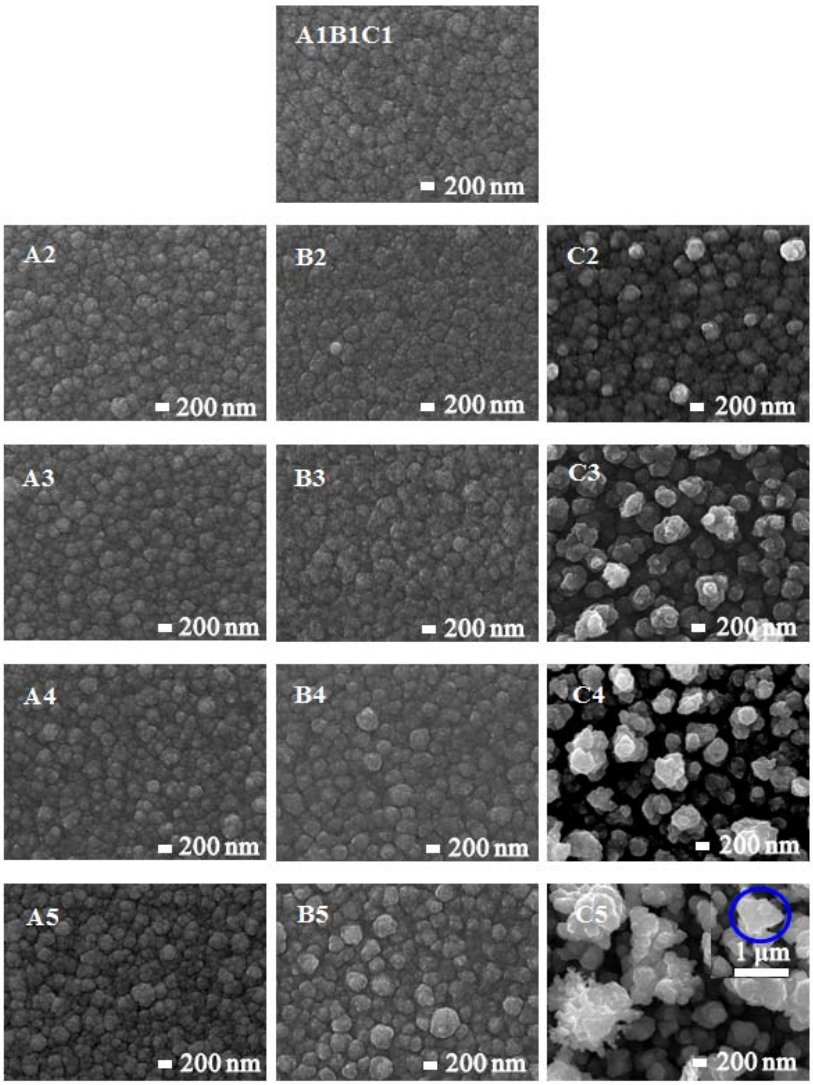

Fig. 3. SEM images of CZT films electrodeposited from electrolyte solutions containing different concentrations of metal ions; Cu (II) (A series), Zn (II) (B series), and Sn (II) (C series)

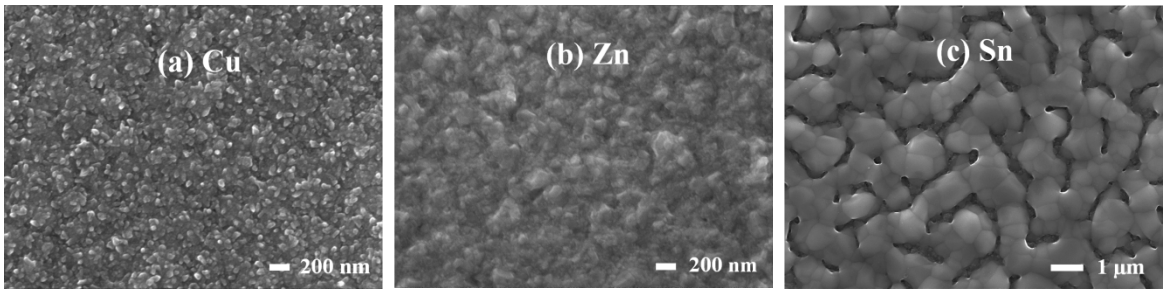

Fig. 4. SEM images of electrodeposited individual metal (a) Cu, (b) Zn and (c) Sn on CZT/Mo/SLG substrate

nucleation mechanism associated with the metal Cu, Zn and Sn respectively in the electrodeposited film. In order to clarify this, the morphology of the films of copper, tin and zinc electrodeposited on a CZT/Mo/SLG substrate separately was investigated. Mo/SLG was not used as substrate for the deposition because it was found that Zn could not be electrodeposited on the surface of Mo/SLG under the reduction potential used. The results show that the average particle size of the film with copper is around 40 nm (Fig. 4a) and that of zinc varies from several nanometers to a few hundred nanometers (Fig. 4b) while the film with tin is composed of micrometer sized islands composed of few hundred nanometer crystals (Fig. 4c)**.** This confirms the larger nucleation size of tin compared to copper and zinc. The different morphologies of the films in Fig. 4 infer that the morphologies of Cu_6Sn_5 and Cu_5Zn_8 alloys should be indirectly affected by the nucleation size of each metal copper and zinc and tin. Obviously, tin has the most significant influence on morphology of the CZT film. The increase of tin content (Fig. 1c) made the film rougher and more porous as seen in Fig. 3 (A1B1C1 - C5). The XRD pattern in Fig. 2g shows the tin crystal grows along the preferred directions of (020)**.** This is also supported by the plate - like crystals formed in the film as marked by a blue circle in the inserted plot in Fig. 3(C5).

3.4 Chronoamperometry characteristic (*i-t*) curve

The chronoamperometry characteristic (*i-t*) curve for the electrochemical deposition of CZT films can also tell the changes of interface between the deposited metal film and the electrolyte solution during the deposition process[37]. The *i-t* curves of the CZT films deposited using different electrolyte solutions are showed in Fig. 5 (a, b and c). As can be seen, the cathodic current density decreases rapidly at the initial stage (about the first 50s for A1B1C1) of the deposition. This is due to the decrease of the concentrations of metal ions in the vicinity of electrode surface caused by electrochemical reduction. After this, the current becomes stable. The *i-t* curve of each metal ion concentration shows different features. In the case of varying the concentration of Cu (II), all the *i-t* curves show a similar trend with the cathodic current becoming constant after 50 s as shown in Fig. 5a, suggesting a constant surface area of the films during the deposition. This is in agreement with the similar morphologies of the films with different concentrations of Cu (II) shown in Fig. 3 (A1B1C1 - A5). However, for the deposition with different concentrations of Zn (II) in the electrolyte solution, the cathodic current at the plateau region increases with the increase of Zn (II) concentration as shown in

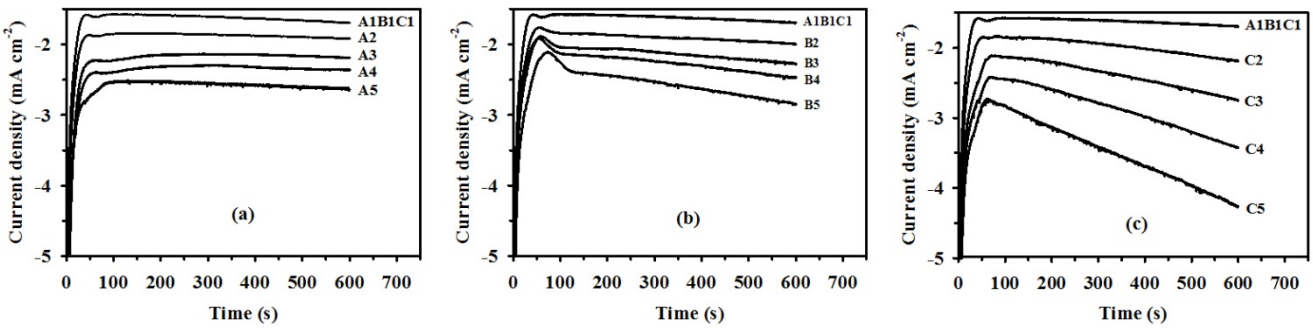

Fig. 5. Comparison of the *i – t* curves for the electrodeposition of CZT films with different concentrations of (a) Cu (II), (b) Zn (II) and (c) Sn (II)

Fig. 5b. This indicates the enhancement of the surface area of the deposited films, which is also consistent with the more rough surface morphology of the film shown in the Fig. 3 (A1B1C1 - B5). It should be noted that significant peaks (Fig. 5b) are observed in the *i-t* curves at the deposition time between 30 s - 100 s for different Zn (II) concentrations, and the peak intensity increases with the increasing concentration of Zn (II). This is attributed to the fact that the reduction of Zn (II) does not occur until sufficient CuSn are present on the surface of the Mo. This appears to occur at 30 – 60 s and is speculated to be due to a lack of reduction ability of Zn (II) on Mo substrate at the voltage. [Fig. S2, supplementary information] Remarkably, with the increase of Sn (II) concentration, the cathodic current at the plateau region increases rapidly and cannot reach a steady value at all as illustrated in Fig. 5c. This is ascribed to the enhanced surface area of the films as a result of the formation of porous structured films as shown in Fig. 3 (A1B1C1 – C5). Nevertheless, a common trend of the increased cathodic currents in the plateau region with the increasing concentration of each metal ion has been observed in all the electrolyte solutions (Fig. 5, a b and c). It suggests the deposition current is dependent on the concentration of each metal ion.

3.5 Characterization of CZTS film

A CZTS film with copper-poor (Cu/(Zn + Sn) ≈ 0.8) and zinc-rich (Zn/Sn≈1.2) composition has been reported to benefit the performance of solar cells[38, 39]. Therefore, it is important to control the contents of copper, zinc and tin in the CZT precursor film in order to fabricate CZTS films with desired composition. As shown above, this can be achieved by finely tuning the concentration of the metal ions in the electrolyte solution because the deposition is controlled by diffusion limited mass transfer. By optimization of the concentrations of the metal ions, a CZT film with composition (atomic ratio) of Cu/(Zn + Sn) = 0.69, Zn/Sn = 1.02 was deposited from an aqueous electrolyte solution containing 13.0 mM $CuSO_4$•$5H_2O$, 12.0 mM $ZnSO_4$•$7H_2O$ and 10.0 mM $SnSO_4$ with 200 mM $Na_3C_6H_5O_7$•$2H_2O$. The thickness of the deposited CZT film is 0.83 µm according to the measurement of cross-sectional SEM image (Fig. 6a). The film is uniformly composed of spherical

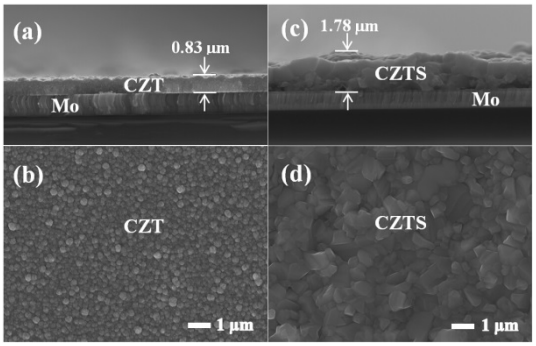

Fig. 6. SEM cross sectional and surface images of optimal CZT film (a and b) and corresponding CZTS film (c and d)

crystallites with size 200 nm (Fig. 6b) and is well adhered to the Mo/SLG substrate. The CZT film was transformed into CZTS through a high temperature sulfurization process at 550 °C for 30 min. The CZTS thin film had the composition (atomic ratio) of Cu/(Zn + Sn) = 0.74, Zn/Sn = 1.33 and S/(Cu+ Zn+ Sn) = 1.05 based on EDS measurement, which falls in the desired compositional range of CZTS films for high performance solar cells. It is found that the ratios of Cu/(Zn + Sn) and Zn/Sn in the CZTS film are higher than the ratios in corresponding CZT film. This is attributed to the loss of tin during the high temperature sulfurization process[40, 41]. The thickness of the CZTS film is 1.78 µm and large polycrystalline grains 0.3 – 1.0 µm can be seen in the compact CZTS film, as shown in Fig. 6c and 6d.

Moreover, the crystal structure of the CZTS film adopts kesterite phase (JCPDS 01 - 075 - 4122) as confirmed by the XRD pattern shown in Fig. 7a. Nevertheless, XRD alone cannot rule out the existence of secondary phases such as Cu_2SnS_3 and cubic ZnS in the film because these materials have similar XRD patterns with CZTS[42]. Hence Raman spectroscopy was used to distinguish these potential impurities from that of CZTS. Herein, both 532 nm and 785 nm laser were applied as excitation source in the Raman measurement. The Raman

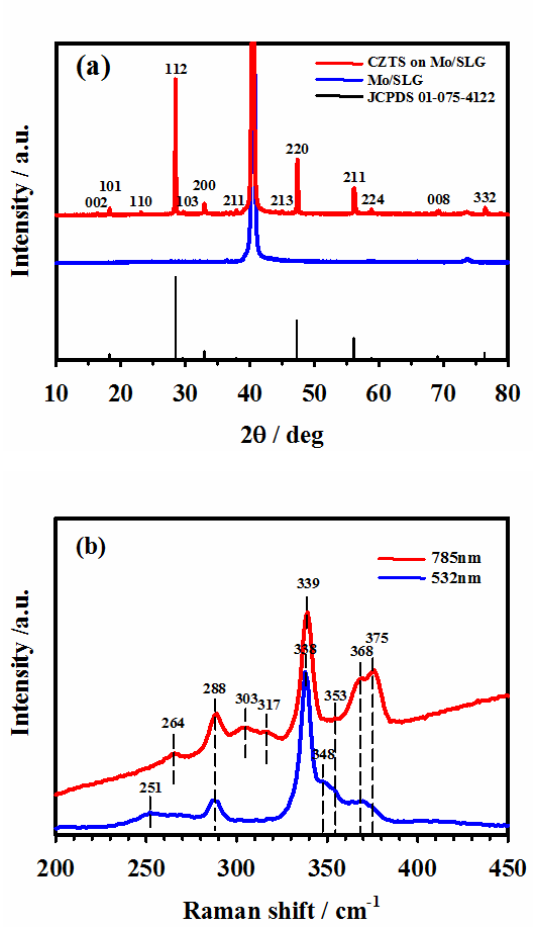

Fig. 7. (a) XRD pattern and (b) Raman spectra of the optimal CZTS film

peaks in Fig. 7b shows that no peaks due to Cu_2SnS_3 are observed. However, cubic ZnS phase may exist in the film

because the characteristic scattering peak of ZnS at around 350 cm^{-1} is observed in the Raman spectrum with 785 nm laser excitation although the intensity of the peak (located at 353 cm^{-1}) is quite weak[43]. The other peaks in both spectra can be assigned to the Raman scattering of kieserite CZTS that have been reported previously[43, 44] . Compared to the spectrum measured by 532 nm laser excitation, more peaks were detected by the 785 nm laser. This is attributed to the effect of vibration resonance because the 785 nm excitation is close to the bandgap (1.5 eV) of CZTS.

3.6 Performance of CZTS solar cell

The performance of the thin film solar cell using the CZTS film under the illumination of 100 mW cm^{-2} (AM 1.5) is shown in Fig. 8. The solar cell shows an energy conversion efficiency of 2.15% with J_{sc} = 11.16 mA cm^{-2}, V_{oc} = 0.47 V and *ff* = 0.47. All these characteristic parameters are lower than those reported (η = 3.74%, *Jsc* = 13.4 mA cm^{-2}, *Voc* = 0.595 and *ff* = 0.47) in the highest efficiency solar cell made by co-electrodeposition method[24]. Jiang et al[18] have shown that preheating treatment can significantly improve the performance of solar cells made from electrodeposited stacked metal layers precursor films. Similar effect would be expected for the film made by co-electrodeposition. We've noticed that a preheating treatment of CZT film was employed in the work of the high efficiency co-electrodeposited CZTS solar cells[24] before the CZT film was sulfurized to form CZTS while no such procedure was used in our work. Thus the lower performance of the solar cell in our work could be related with the different thermal treatment used in the film fabrication. The series resistance (R_s = 22.69 Ω cm^2) and shunt-resistance (R_{sh} = 290.13 Ω cm^2) of the solar cell are shown in Fig.8. It is well known that a high efficient solar cell requires low R_s and high R_{sh}. The relatively high R_s value of 22.69 Ω cm^2 in this work compared to what has been reported in a high efficiency solar cell[14] (R_s = 4.10 Ω cm^2 and η = 7.3%) should be one of the factors for the lower *ff* in the present

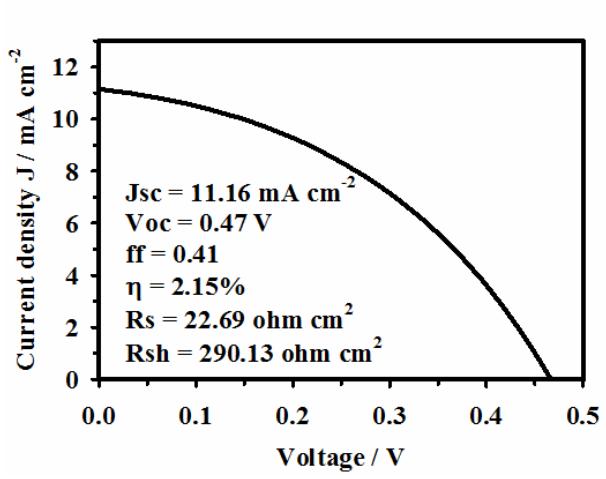

Fig. 8. *J-V* plot of the CZTS solar cell

work. The higher R_s is probably a result of the voids and small sized crystals formed in the bottom layer of the CZTS film (Fig.6c). These voids may also work as recombination centers to cause lower J_{sc} and V_{oc}, and further decrease the conversion efficiency of the solar cell.

4. Conclusions

The effects of the concentrations of Cu (II), Zn (II) and Sn (II) ions in the electrolyte solution on the composition, material phases and morphologies of the electrodeposited CZT films were systematically studied in this work. It has been found that the content of metal in the CZT films was linearly dependent on the concentration of the corresponding metal ion in the electrolyte solution. Moreover, it has been found that the increase of Cu (II) concentration in the solution facilitated the formation of Cu_6Sn_5 and Cu_5Zn_8 alloy phases. However, the increase of Zn (II) and Sn (II) concentration had no influence on the formation of these alloys. The investigation of the film by SEM has shown that Cu (II) had no effect on the CZT film morphology while Zn (II) increased both crystal size and surface roughness of the film. Sn (II) showed the most dramatic effect on the CZT film morphology with the formation of porous film. The different morphological dependence with different metals was attributed to the different electrochemical nucleation sizes of the metals. The changes of the surface property of the CZT with different content of metals were also confirmed by chronoamperometry characteristic (*i-t*) deposition curves. Through tailoring concentrations of the metal precursor salts in the electrolyte solution, a copper-poor and zinc-rich CZTS film with kesterite structure was synthesized and the corresponding solar cell exhibited an energy conversion efficiency of 2.15% under the illumination intensity of 100 mW cm^{-2}.

Acknowledgments

T. Hreid acknowledges the PhD scholarship program of Queensland University of Technology. H.W thanks the financial support from Australian Research Council (ARC) Future Fellowship (grant No: FT120100674).

Supplementary information

Supplementary date associated with this article can be found in Fig. S1 and S2 as mentioned in the main text.

References

1. S. Abermann, *Solar Energy*, 2013, **94**, 37-70.
2. H. Wang, *International Journal of Photoenergy*, 2011, DOI: 801292.
3. K. Ramasamy, M. A. Malik and P. O'Brien, *Chemical Communications*, 2012, **48**, 5703-5714.
4. J. Tao, J. He, K. Zhang, J. Liu, Y. Dong, L. Sun, P. Yang and J. Chu, *Materials Letters*, 2014, **135**, 8-10.
5. J. Tao, J. Liu, J. He, K. Zhang, J. Jiang, L. Sun, P. Yang and J. Chu, *RSC Advances*, 2014, **4**, 23977-23984.

6. A. Brenner, *Electrodeposition of alloys: principles and practice*, Elsevier, 2013.
7. J. J. Scragg, D. M. Berg and P. J. Dale, *Journal of Electroanalytical Chemistry*, 2010, **646**, 52-59.
8. H. Araki, Y. Kubo, K. Jimbo, W. S. Maw, H. Katagiri, M. Yamazaki, K. Oishi and A. Takeuchi, *physica status solidi (c)*, 2009, **6**, 1266-1268.
9. J. J. Scragg, P. Dale and L. M. Peter, *Thin Solid Films*, 2009, **517**, 2481-2484.
10. Y. Lin, S. Ikeda, W. Septina, Y. Kawasaki, T. Harada and M. Matsumura, *Solar Energy Materials and Solar Cells*, 2014, **120**, 218-225.
11. R. Kondrotas, R. Juškėnas, A. Naujokaitis, A. Selskis, R. Giraitis, Z. Mockus, S. Kanapeckaitė, G. Niaura, H. Xie and Y. Sánchez, *Solar Energy Materials and Solar Cells*, 2015, **132**, 21-28.
12. L. Vauche, J. Dubois, A. Laparre, F. Mollica, R. Bodeux, S. Delbos, C. M. Ruiz, M. Pasquinelli, F. Bahi and T. G. de Monsabert, *physica status solidi (a)*, 2014, **211**, 2082-2085.
13. Y. Zhang, C. Liao, K. Zong, H. Wang, J. Liu, T. Jiang, J. Han, G. Liu, L. Cui and Q. Ye, *Solar Energy*, 2013, **94**, 1-7.
14. J. Li, T. Ma, M. Wei, W. Liu, G. Jiang and C. Zhu, *Applied Surface Science*, 2012, **258**, 6261-6265.
15. L. Guo, Y. Zhu, O. Gunawan, T. Gokmen, V. R. Deline, S. Ahmed, L. T. Romankiw and H. Deligianni, *Progress in Photovoltaics: Research and Applications*, 2013.
16. S. Ahmed, K. B. Reuter, O. Gunawan, L. Guo, L. T. Romankiw and H. Deligianni, *Advanced Energy Materials*, 2012, **2**, 253-259.
17. J. O. Jeon, K. D. Lee, L. Seul Oh, S. W. Seo, D. K. Lee, H. Kim, J. h. Jeong, M. J. Ko, B. Kim and H. J. Son, *ChemSusChem*, 2014, **7**, 1073-1077.
18. F. Jiang, S. Ikeda, T. Harada and M. Matsumura, *Advanced Energy Materials*, 2014, **4**.
19. J. J. Scragg, D. M. Berg and P. J. Dale, *Journal of Electroanalytical Chemistry*, 2010, **646**, 52-59.
20. P. K. Sarswat, M. Snure, M. L. Free and A. Tiwari, *Thin solid films*, 2011.
21. H. Araki, Y. Kubo, A. Mikaduki, K. Jimbo, W. S. Maw, H. Katagiri, M. Yamazaki, K. Oishi and A. Takeuchi, *Solar Energy Materials and Solar Cells*, 2009, **93**, 996-999.
22. J. J. Scragg, P. J. Dale and L. M. Peter, *Electrochemistry Communications*, 2008, **10**, 639-642.
23. A. Ennaoui, M. Lux-Steiner, A. Weber, D. Abou-Ras, I. Kötschau, H. W. Schock, R. Schurr, A. Hölzing, S. Jost and R. Hock, *Thin solid films*, 2009, **517**, 2511-2514.
24. K. Gurav, S. Pawar, S. W. Shin, G. Agawane, P. Patil, J.-H. Moon and J. H. Kim, *Applied Surface Science*, 2013.
25. Y. Li, T. Yuan, L. Jiang, Z. Su and F. Liu, *Journal of Alloys and Compounds*, 2014, **610**, 331-336.
26. Y. Li, T. Yuan, L. Jiang, F. Liu, Y. Liu and Y. Lai, *Journal of Materials Science: Materials in Electronics*, 2015, **26**, 204-210.
27. K. D. Lee, S.-W. Seo, D.-K. Lee, H. Kim, J.-h. Jeong, M. J. Ko, B. Kim, D. H. Kim and J. Y. Kim, *Thin Solid Films*, 2013, **546**, 294-298.
28. C. Gougaud, D. Rai, S. Delbos, E. Chassaing and D. Lincot, *Journal of The Electrochemical Society*, 2013, **160**, D485-D494.
29. M. Slupska and P. Ozga, *Electrochimica Acta*, 2014, **141**, 149-160.
30. R. Juškėnas, S. Kanapeckaitė, V. Karpavičienė, Z. Mockus, V. Pakštas, A. Selskienė, R. Giraitis and G. Niaura, *Solar Energy Materials and Solar Cells*, 2012.
31. L. Picincu, D. Pletcher and A. Smith, *Journal of applied electrochemistry*, 2001, **31**, 387-394.
32. L. Picincu, D. Pletcher and A. Smith, *Journal of applied electrochemistry*, 2001, **31**, 395-402.
33. M. F. de Carvalho, E. P. Barbano and I. A. Carlos, *Surface and Coatings Technology*, 2015, **262**, 111-122.
34. K. Gurav, S. Pawar, S. W. Shin, G. Agawane, P. Patil, J.-H. Moon, J. Yun and J. H. Kim, *Applied Surface Science*, 2013, **283**, 74-80.
35. X. He, H. Shen, W. Wang, J. Pi, Y. Hao and X. Shi, *Applied Surface Science*, 2013, **282**, 765-769.
36. J. Li, Y. Zhang, H. Wang, L. Wu, J. Wang, W. Liu, Z. Zhou, Q. He and Y. Sun, *Solar Energy Materials and Solar Cells*, 2015, **132**, 363-371.
37. A. P. O'Mullane, S. J. Ippolito, Y. M. Sabri, V. Bansal and S. K. Bhargava, *Langmuir*, 2009, **25**, 3845-3852.
38. S. Bag, O. Gunawan, T. Gokmen, Y. Zhu, T. K. Todorov and D. B. Mitzi, *Energy & Environmental Science*, 2012, **5**, 7060-7065.
39. S. Chen, A. Walsh, X. G. Gong and S. H. Wei, *Advanced Materials*, 2013.
40. J. J. Scragg, J. T. Watjen, M. Edoff, T. Ericson, T. Kubart and C. Platzer-Björkman, *Journal of the American Chemical Society*, 2012, **134**, 19330-19333.
41. J. J. Scragg, T. Ericson, T. Kubart, M. Edoff and C. Platzer-Björkman, *Chemistry of Materials*, 2011, **23**, 4625-4633.
42. V. T. Tiong, T. Hreid, G. Will, J. Bell and H. Wang, *Science of Advanced Materials*, 2014, **6**, 1467-1474.
43. P. Fernandes, P. Salomé and A. Da Cunha, *Journal of Alloys and Compounds*, 2011, **509**, 7600-7606.
44. J. J. Scragg, L. Choubrac, A. Lafond, T. Ericson and C. Platzer-Björkman, *Applied Physics Letters*, 2014, **104**, 041911.